Macromolecules

Article

Cite This: Macromolecules 2018, 51, 6190−6201

pubs.acs.org/Macromolecules

Photoinitiated Polymerization-Induced Self-Assembly in the Presence of Surfactants Enables Membrane Protein Incorporation into Vesicles

Spyridon Varlas,[†,§] Lewis D. Blackman,[†] Heather E. Findlay,[∥] Eamonn Reading,[∥] Paula J. Booth,[∥] Matthew I. Gibson,[†,‡] and Rachel K. O'Reilly*[,§]

[†]Department of Chemistry and [‡]Warwick Medical School, University of Warwick, Gibbet Hill Road, CV4 7AL Coventry, U.K.
[§]School of Chemistry, University of Birmingham, B15 2TT Birmingham, U.K.
[∥]Department of Chemistry, King's College London, Britannia House, 7 Trinity Street, SE1 1DB London, U.K.

Supporting Information

ABSTRACT: Photoinitiated polymerization-induced self-assembly (photo-PISA) is an efficient approach to predictably prepare polymeric nanostructures with a wide range of morphologies. Given that this process can be performed at high concentrations and under mild reaction conditions, it has the potential to have significant industrial scope. However, given that the majority of industrial (and more specifically biotechnological) formulations contain mixtures of polymers and surfactants, the effect of such surfactants on the PISA process is an important consideration. Thus, to expand the scope of the methodology, the effect of small molecule surfactants on the PISA process, specifically for the preparation of unilamellar vesicles, was investigated. Similar to aqueous photo-PISA findings in the absence of surfactant molecules, the originally targeted vesicular morphology was retained in the presence of varying concentrations of non-ionic surfactants, while a diverse set of lower-order morphologies was observed for ionic surfactants. Interestingly, a critical micelle concentration (CMC)-dependent behavior was detected in the case of zwitterionic detergents. Additionally, tunable size and membrane thickness of vesicles were observed by using different types and concentration of surfactants. Based on these findings, a functional channel-forming membrane protein (OmpF porin), stabilized in aqueous media by surfactant molecules, was able to be directly inserted into the membrane of vesicles during photo-PISA. Our study demonstrates the potential of photo-PISA for the direct formation of protein−polymer complexes and highlights how this method could be used to design biomimicking polymer/surfactant nanoreactors.

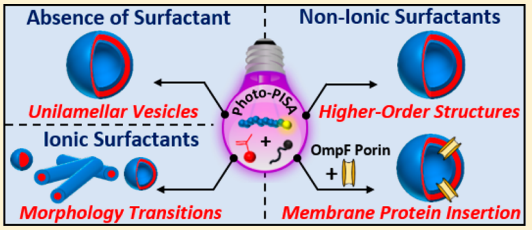

INTRODUCTION

Small molecule surfactants, also known as surface-active agents, have been extensively utilized as wetting agents, emulsifiers, plasticizers, etc., in cleaning, food, oil, and textile industry.[1,2] Self-assembled amphiphilic polymer aggregates (macromolecular counterparts of surfactants) have also accumulated significant interest as they exhibit greater stability compared to surfactant assemblies due to their superior mechanical and physical properties.[3,4] Today, mixed polymer−surfactant formulations that coassemble at a certain critical aggregation concentration are also used in various household, personal care, and other industrial and biotechnological applications.[5,6] Hence, the need to understand the effect of small molecule surfactants on polymeric assemblies and the interaction of such complex systems is increasingly required.

In an early report by Wesley et al., the interaction of anionic surfactant sodium dodecyl sulfate (SDS) with poly(2-(dimethylamino)ethyl methacrylate) (PDMAEMA) homopolymer chains was investigated.[7] Small-angle neutron scattering revealed that the presence of polymer induced the micellization of the surfactant at concentrations below its CMC value, an observation also shown in a different study by Diamant and Andelman.[8] Pata et al. investigated the effect of non-ionic surfactant Triton X-100 on poly(ethylene oxide)-*b*-poly(ethyl ethylene) and poly(ethylene oxide)-*b*-poly(butadiene) diblock copolymer vesicles.[9] Higher resistance to membrane dissolution was achieved upon increasing the bilayer thickness of such vesicles. Armes and co-workers prepared epoxy-functional diblock copolymer vesicles by aqueous RAFT dispersion polymerization.[10] Cross-linking of the membrane of the vesicles was achieved, and the stability of vesicles toward externally added amounts of small molecule surfactants of different nature (i.e., ionic and neutral) was then studied. The non-cross-linked vesicles could tolerate the presence of non-ionic surfactants, while they were easily disrupted upon exposure to ionic species (surfactant-induced dissociation). On the contrary, the cross-linked vesicles remained stable in the presence of both non-ionic and ionic surfactants. More recently, Atanase et al. studied the micellization behavior of poly(butadiene)-*b*-poly(2-vinylpyridine)-*b*-poly(ethylene

Received: May 9, 2018
Revised: July 7, 2018
Published: August 6, 2018

DOI: 10.1021/acs.macromol.8b00994
Macromolecules 2018, 51, 6190−6201

oxide) (PB-*b*-P2VP-*b*-PEO) triblock copolymers as a function of pH and SDS concentration.[11] SDS addition led to a noticeable decrease of particles' size, indicating the development of strong hydrophobic interactions between SDS and P2VP and the formation of surfactant−polymer complexes. Importantly, phospholipid/block copolymer hybrid vesicles (lipo-polymersomes) have been also studied in depth because of their similarity, in terms of thickness and hydrophobicity, to cell membranes and their advantages of combining the best features of both species.[12−15]

Over recent years, polymerization-induced self-assembly (PISA) has become a widely utilized and efficient synthetic methodology to produce block copolymer nano-objects of controlled size, morphology, and tunable properties.[16,17] Owing to the fact that traditional block copolymer self-assembly methods are mostly conducted at low polymer concentrations (≤1% w/w) and in almost all cases require further postpolymerization processing, which makes it difficult to implement on a large scale, PISA has become an alternative one-pot route to reproducibly prepare nano-objects at high concentrations (10−50% w/w).[18,19] Controlled radical polymerization techniques such as nitroxide-mediated polymerization (NMP),[20] atom-transfer radical polymerization (ATRP),[21] and reversible addition−fragmentation chain-transfer (RAFT) polymerization[22−25] have been mainly applied in this process, although RAFT polymerization is still the most popular method owing to its high versatility and broad applicability. Typically, in RAFT-mediated dispersion PISA, a solvophilic macromolecular chain transfer agent (macro-CTA) is chain-extended using miscible monomers such that the growing second block gradually becomes insoluble, which drives *in situ* self-assembly to form amphiphilic diblock copolymers. These generate a set of higher-order polymeric nanostructures with morphologies that evolve by varying the degree of polymerization (DP) and solids concentration.[26]

Nevertheless, research toward bio-related or stimuli-responsive nanomaterials produced by aqueous PISA is currently limited. This is mainly attributed to the elevated reaction temperatures required for most thermally initiated aqueous PISA formulations that can lead to denaturation of delicate biomolecules such as proteins, enzymes, or antibodies.[27] Recently, an increasing number of studies based on aqueous visible-light-initiated PISA (photo-PISA) at ambient temperatures have been reported, showing great promise in the design and preparation of novel materials of particular biotechnological and biomedical interest.[28−34]

The design of facile and mild routes for the preparation of well-defined single-phase vesicles by photo-PISA is of great interest as it allows for the development of cargo-loaded nanocarriers in a single step, which is especially important for the encapsulation of delicate biomolecules. To date, several studies on the encapsulation of hydrophilic proteins and enzymes inside polymeric vesicles via one-pot aqueous photo-PISA under mild reaction conditions (i.e., low temperature, visible light, and aqueous media) have been reported.[27,28,35−38] On the contrary, conventional methods[39,40] used for the insertion of hydrophobic and/or amphiphilic (macro)-molecules (e.g., drugs, enzymes, receptors, and membrane proteins) into vesicles are not often appropriate for delicate and very hydrophobic biomolecules. Indeed, for very hydrophobic biomolecules (e.g., membrane proteins), such uptake into vesicles cannot be achieved without the presence of solubilizing agents such as surfactants.[41−44] The incorporation of membrane proteins (specifically channel proteins, such as OmpF) into vesicles has been pioneered by Meier, Palivan, and co-workers, who have demonstrated such nanoconstructs as synthetic cell mimics (organelles).[40,45,46] To further broaden the scope of the synthesis of such membrane protein−vesicle complexes, we were interested in exploring photo-PISA to allow for uptake into the hydrophobic domain formed during polymerization (given its mild, tolerant, and scalable conditions).

To achieve this, we first explored the interaction and effect of small molecule surfactants of different critical micelle concentration (CMC) values and nature (i.e., neutral, ionic, and zwitterionic), commonly used in various biotechnological applications, on the self-assembly process of a poly(ethylene glycol)-*b*-poly(2-hydroxypropyl methacrylate) (PEG-*b*-PHPMA) block copolymer system developed by aqueous photo-PISA, while always targeting unilamellar vesicles (ULVs) as the desired final morphology. We were able to demonstrate that mixed block copolymer/surfactant vesicles with tunable size and membrane thickness could be obtained upon appropriate usage of different types and concentrations of surfactants. On the basis of these findings, we then moved toward using these conditions for incorporation of the pore-forming outer membrane protein F (OmpF), which is insoluble in water, requires the addition of surfactants for solubilization, and hence is challenging to incorporate directly into polymeric self-assemblies. This was achieved by conducting photo-PISA in the presence of OmpF, which was first stabilized by a non-ionic surfactant to allow for direct reconstitution into the membrane of the vesicles, as demonstrated by their enhanced permeability. We propose that this demonstration highlights the potential application of photo-PISA methodology, in the presence of surfactants, for insertion of challenging hydrophobes and hence could contribute significantly to the further development of biomembrane-mimicking nanoreactors.

RESULTS AND DISCUSSION

Based on findings from other related literature reports by Armes'[47] and Zhang's groups,[28] and more recently by our group[24,36] for similar PISA systems, a poly(ethylene glycol) macro-chain-transfer agent with same molecular weight (5.0×10^3 g mol^{-1}, DP = 113) as the one used in these studies was first synthesized. This was achieved through esterification of an acid functionalized chain-transfer agent (CEPA CTA) with a poly(ethylene glycol) monomethyl ether homopolymer (PEG_{113}-OH) by DCC coupling chemistry (esterification efficiency = 93%; see the Supporting Information for experimental details).

This water-soluble macro-CTA was then chain-extended under dispersion polymerization conditions using a water-miscible monomer, 2-hydroxypropyl methacrylate (HPMA), as the core-forming block. It should be noted that the monomer was a mixture of two isomers: 2-hydroxypropyl methacrylate (major, 75 mol %) and 2-hydroxyisopropyl methacrylate (minor, 25 mol %). Aqueous RAFT-mediated photo-PISA of HPMA occurred upon 405 nm visible-light irradiation of the solution at 37 °C under a N_2 atmosphere for the synthesis of PEG-*b*-PHPMA nano-objects (Scheme S1), and complete monomer conversion (>99%) was achieved after 2 h of reaction, as determined by ^{1}H NMR spectroscopy (Figure S1). It should be mentioned that the polymerization process was

DOI: 10.1021/acs.macromol.8b00994
Macromolecules 2018, 51, 6190−6201

Scheme 1. (A) Schematic Illustration Showing the Obtained PEG_{113}-*b*-$PHPMA_{400}$ Nano-Object Morphologies after Photo-PISA in Deionized Water and in Different Type Surfactant Solutions at Concentrations Equal to or Higher than the Critical Micelle Concentration (CMC) of Each Surfactant; (B) Summary of Chemical Structures and Main Characteristics of the Surfactants Used in the Present Study (CMC Values in Water As Reported in the Literature)

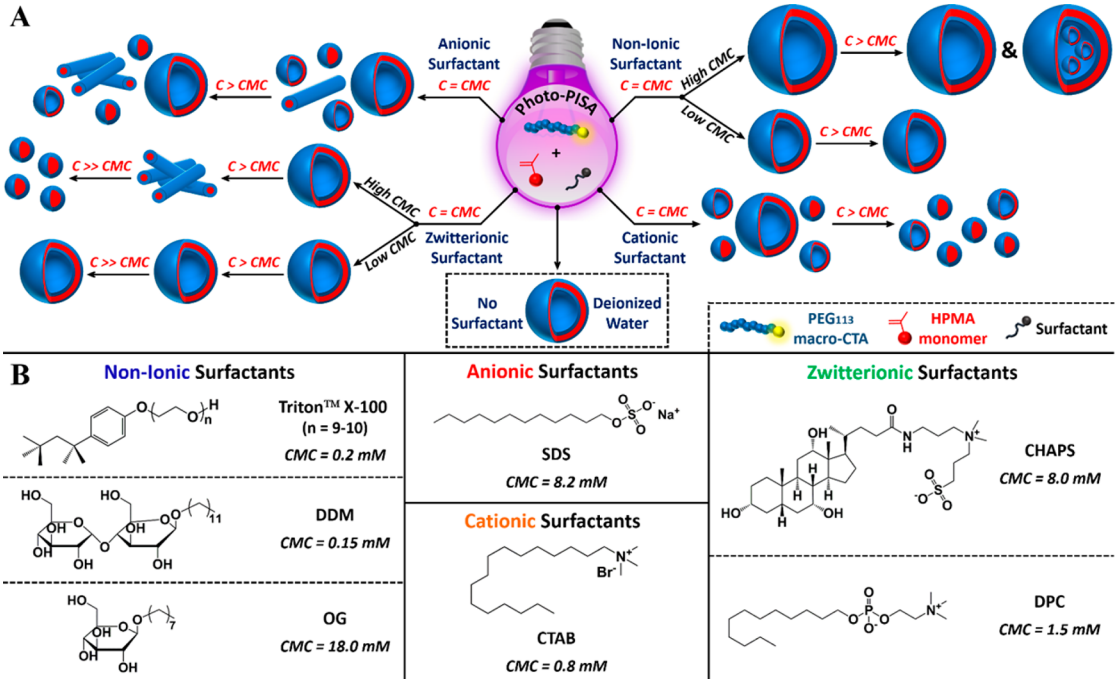

promoted in the absence of an initiator or catalyst, following the well-documented "photoiniferter" mechanism.[48]

Based on the morphologies diagram for photo-PISA of PEG_{113}-*b*-$PHPMA_x$ in deionized (DI) water recently reported by our group,[24] well-defined unilamellar vesicles (ULVs) were formed when targeting DP_{PHPMA} = 400 at 10 wt % HPMA (11 wt % solids content) (Scheme 1A). SEC analysis in DMF of a lyophilized PEG_{113}-*b*-$PHPMA_{400}$ sample confirmed the successful chain extension of HPMA and revealed the controlled character of the photo-PISA process as indicated by the relatively narrow molecular weight distribution determined ($M_{n,SEC\ RI}$ = 80.1 × 10^3 g mol^{-1}, $Đ_{M\ RI}$ = 1.25) (Table S1).

Dry-state stained TEM imaging revealed the successful formation of ULVs of uniform size, while DLS analysis also confirmed a unimodal particle size distribution with hydrodynamic diameter (D_h) in the range 350−400 nm (Figure S2). The shape, size, and unilamellar character of the developed PEG_{113}-*b*-$PHPMA_{400}$ vesicles in solution were confirmed by cryo-TEM imaging, while their average membrane thickness was also determined as 26.8 ± 3.4 nm (Figure S3). These findings were in good agreement with our previously reported characterization results for the same system, suggesting the facile reproducibility of the photo-PISA process.[24,36] Zeta potential measurements of the prepared vesicles after purification in DI water showed a negative value of −30.5 ± 0.4 mV, mainly attributed to the free −OH groups of the relatively hydrated PHPMA membrane that are not entirely screened by the PEG 5 kDa chains.[49−51] It is also important to mention that the purification process of the particles by centrifugation/resuspension cycles in DI water did not significantly affect any of their characteristics (i.e., shape, size, and zeta potential).

The key aim of this research was to evaluate the impact of small molecule surfactants (detergents) used in various industrial and biotechnological applications, such as solubilizing agents of hydrophobic membrane proteins, on the formulations obtained by photo-PISA. Aqueous photo-PISA reactions for the development of PEG_{113}-*b*-$PHPMA_{400}$ nano-objects were performed in the presence of various surfactants (non-ionic, anionic, cationic, and zwitterionic) with differing CMC values, under the same polymerization conditions described above (Scheme 1). A low-CMC non-ionic surfactant with a hydrophilic oligo(ethylene glycol) head, Triton X-100 (*n* = 9−10), and two non-ionic pyranoside surfactants, *n*-dodecyl *β*-D-maltoside (DDM, low CMC) and octyl *β*-D-glucopyranoside (OG, high CMC), were first studied. Additionally, a model anionic surfactant, sodium dodecyl sulfate (SDS), and a cationic surfactant, cetyltrimethylammonium bromide (CTAB), were also investigated. Notably, the effect of two zwitterionic surfactants, 3-[(3-cholamidopropyl)dimethylammonio]-1-propanesulfonate (CHAPS, high CMC) and *n*-dodecylphosphocholine (DPC, low CMC), on photo-PISA nano-object morphologies was finally assessed. It is worth mentioning that the presence of 10 wt % HPMA in PISA solutions did not significantly alter the CMC value of surfactants, as determined by surface tension analysis (Figure S4). The developed polymer−surfactant hybrid formulations could potentially be utilized for *in situ* incorporation of unstable in aqueous media functional (macro)molecules, such as receptors, peptides, enzymes, membrane proteins, and DNA, and fabrication of biomimetic nanoreactors. The observed PEG_{113}-*b*-$PHPMA_{400}$ diblock copolymer/surfactant morphologies formed by aqueous photo-PISA are schematically summarized in Scheme 1A, while the chemical structures along with the main characteristics of the surfactants used in this study are shown in Scheme 1B.

DOI: 10.1021/acs.macromol.8b00994
Macromolecules 2018, 51, 6190−6201

In all cases, photo-PISA reactions were carried out at three different concentrations of each individual surfactant (i.e., at concentrations equal to each detergent's CMC and also at 10 times lower and 10 times higher concentration levels) for the synthesis of nano-objects for the same block copolymer. Moreover, in cases of non-ionic surfactants Triton X-100 and DDM and zwitterionic CHAPS and DPC additional surfactant concentrations were also investigated due to the wide use of these particular surfactants in numerous biotechnologically relevant applications. Purification of samples was achieved by consecutive centrifugation/resuspension cycles in DI water for the removal of unreacted monomer and excess of non-incorporated surfactant molecules. ^{1}H NMR spectroscopy was used for determination of surfactant incorporation in purified OG and CHAPS samples at 10 × CMC (high-CMC surfactants with visible peaks) (Figure S5). For OG, a surfactant incorporation of 6% was calculated, while a higher surfactant incorporation of 14.5% was calculated in the case of CHAPS.

Molecular Characteristics of Polymer–Surfactant Photo-PISA Formulations. The final monomer conversion after photo-PISA in different surfactant solutions for the synthesis of PEG_{113}-*b*-$PHPMA_{400}$ nano-objects was first determined by ^{1}H NMR spectroscopy. It was found that the reaction times of photo-PISA processes were not significantly affected by the presence of surfactants in the system, with almost quantitative monomer conversions (≥96%) achieved after 2 h of irradiation time in almost all cases (Table S2). The only exception was noticed at [CHAPS] = 160.0 mM (= 20 × CMC), where monomer conversion of 70% was calculated (polymerization repeated in duplicate). This rate retardation could be explained by the inability of monomer to reach the gradually growing copolymer chains due to their high solubilization inside the core of the surfactant micelles at high CHAPS concentration. Repeating the polymerization procedure in the same CHAPS solution for 18 h resulted in >99% conversion. SEC analyses in DMF of purified and lyophilized PEG_{113}-*b*-$PHPMA_{400}$ samples at surfactant concentrations (C_{surf}) equal to CMC proved the relatively controlled character of polymerization in each case (Figure 1). In particular, a minimal M_n increase was observed in almost every polymer/surfactant sample as compared to PEG_{113}-*b*-$PHPMA_{400}$ diblock copolymers formed in DI water, accompanied by a minor $Đ_M$ increase from 1.25 (DI water) to 1.29–1.33 (surfactant solutions). Notably, no major M_n and $Đ_M$ differences were detected between diblock copolymer samples in surfactant species of different nature. SEC eluograms of selected diblock copolymer samples prepared at C_{surf} > CMC revealed that a 10-fold surfactant concentration increase did not result in a further increase of molecular weight and $Đ_M$ values (Figure S6). These findings indicate that the presence of surfactants during photo-PISA did not markedly affect the molecular characteristics of the developed PEG_{113}-*b*-$PHPMA_{400}$ diblock copolymers and reveal the high tolerance of dispersion polymerization process toward different types of surfactants.

On the basis of the SEC results, it can be assumed that all nano-objects' size variations and morphology transitions observed are attributed to the nature and CMC value (i.e., amount) of the surfactant used in each case and not to loss of polymerization control during photo-PISA in different surfactant solutions. Exhaustive DLS analysis of the received PEG_{113}-*b*-$PHPMA_{400}$ photo-PISA formulations before and after purification process was performed to monitor the hydrodynamic diameter (D_h) and polydispersity (PD) changes upon increasing concentration of surfactants. Dry-state stained TEM imaging was used for the observation of the prepared

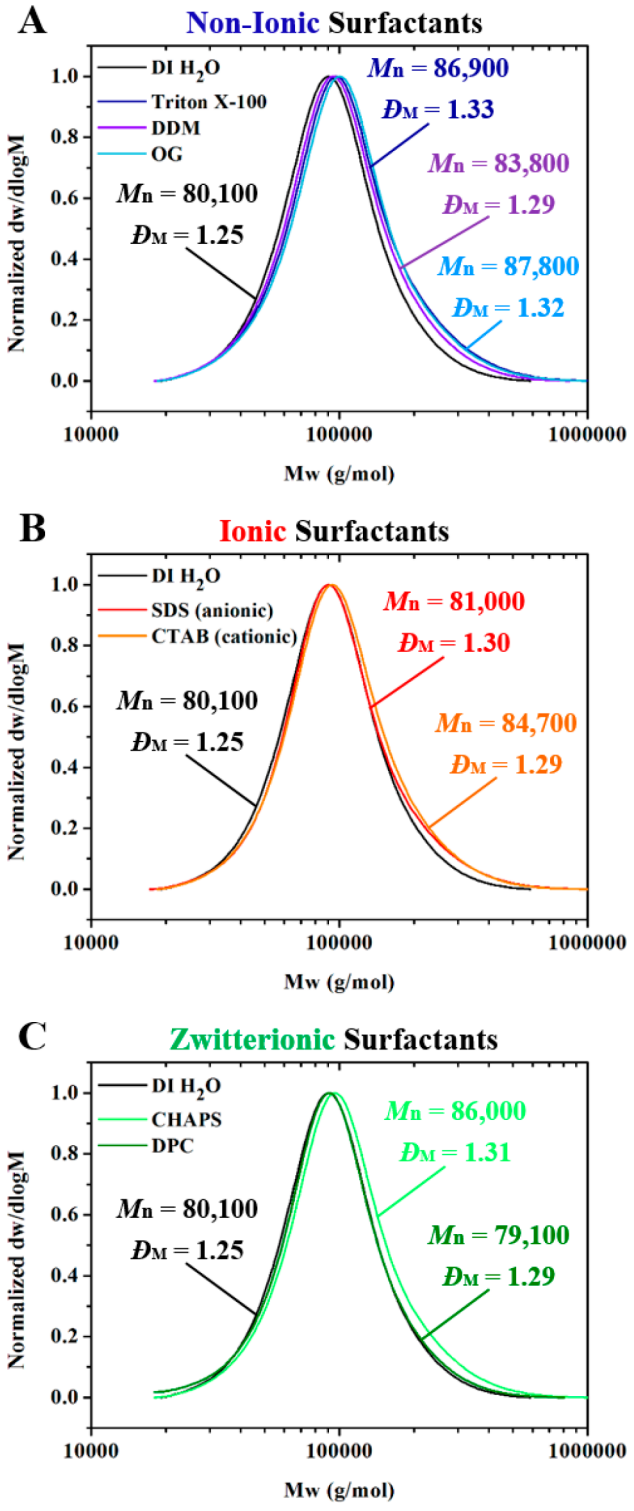

Figure 1. SEC RI molecular weight distributions for PEG_{113}-*b*-$PHPMA_{400}$ diblock copolymers synthesized in the presence of (A) non-ionic, (B) ionic, and (C) zwitterionic surfactants at C_{surf} = CMC in each case along with their corresponding M_n (g mol^{-1}) and $Đ_M$ values calculated from PMMA standards, using 5 mM NH_4BF_4 in DMF as the eluent.

DOI: 10.1021/acs.macromol.8b00994
Macromolecules 2018, 51, 6190–6201

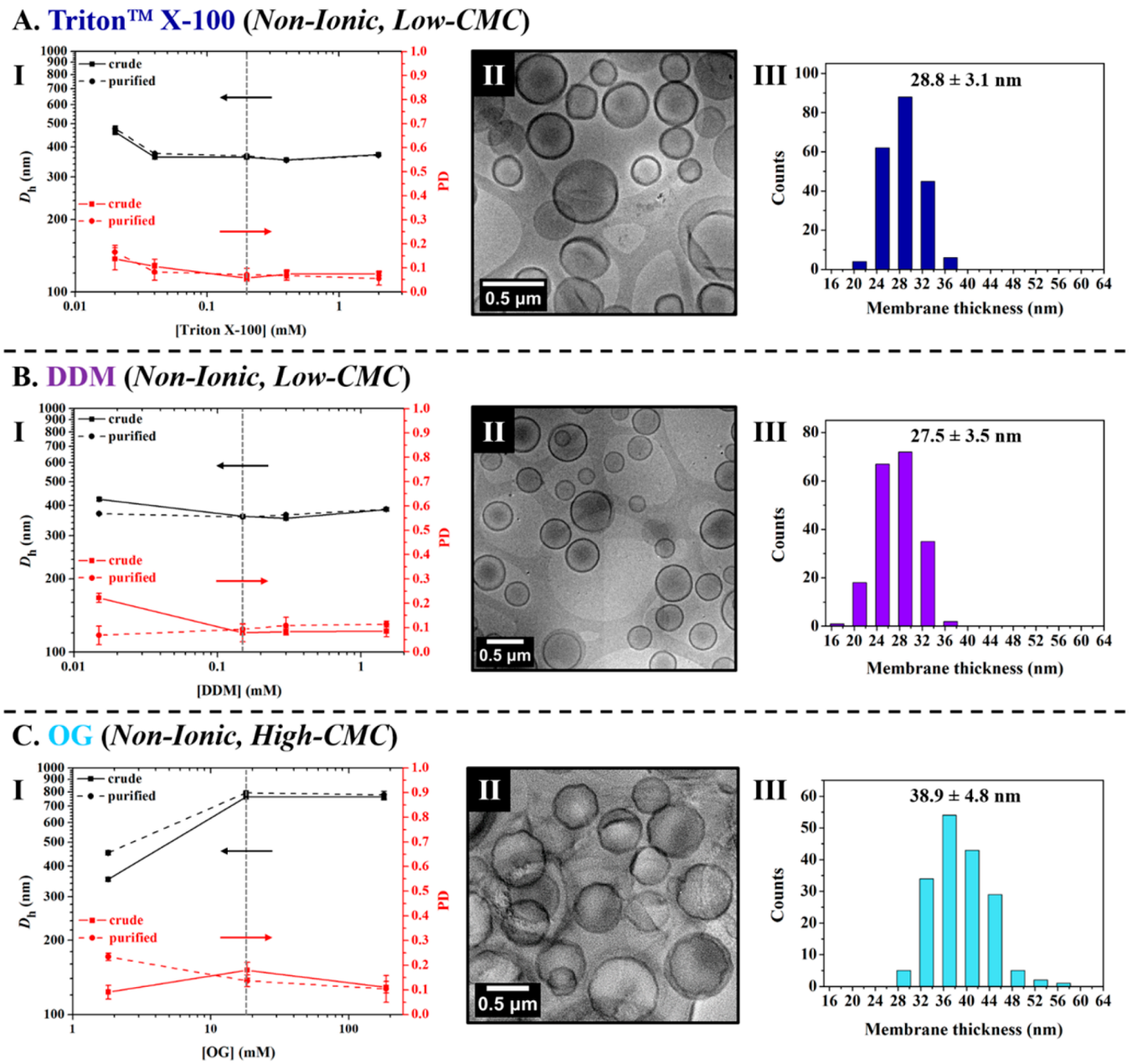

Figure 2. Summary of DLS and cryo-TEM analyses results for PEG_{113}-*b*-$PHPMA_{400}$ diblock copolymer nano-objects developed by aqueous photo-PISA in the presence of non-ionic surfactants Triton X-100 (A), DDM (B), and OG (C). For each individual surfactant: (I) DLS of crude and purified formulations for the monitoring of D_h and PD changes upon increasing surfactant concentration (the error shows the standard deviation from five repeat measurements, while the vertical dashed line indicates the CMC value of each detergent). (II) Representative cryo-TEM images of purified PEG_{113}-*b*-$PHPMA_{400}$ nano-objects formed at C_{surf} = CMC. (III) Distribution of vesicles' membrane thicknesses measured from statistical analysis and calculated average membrane thickness (the error shows the standard deviation from at least 150 particle membranes).

polymer−surfactant nano-object morphologies in each case, while the received purified hybrid nano-objects in solution, formed by photo-PISA at C_{surf} = CMC, were also characterized by cryogenic transmission electron microscopy (cryo-TEM). Additionally, in the case of vesicles, the average membrane thickness was calculated from statistical analysis by measuring at least 150 particle membranes in each sample.

Photo-PISA Nano-Objects Developed in the Presence of Non-Ionic Surfactants. In the case of non-ionic and low-CMC surfactant Triton X-100, it is evident that D_h and PD values were found to be similar to those of original PEG_{113}-*b*-$PHPMA_{400}$ vesicles in DI water, remaining constant for a wide range of surfactant concentrations (Figure 2A-I). Near-identical behavior was noticed for DDM, which is also another low-CMC non-ionic detergent with almost equal CMC value to Triton X-100 (Figure 2B-I). It should also be noted that in these cases the purification process did not affect the D_h or PD values, showing that the nanostructures remain intact after centrifugation/resuspension in DI water. From dry-state TEM imaging, it was observed that spherical unilamellar vesicles (ULVs) of uniform size (350−400 nm) were developed in both cases, analogous to those formed in DI water (Figures S7−S10). Results from cryo-TEM analysis were in good agreement with those received from other characterization

DOI: 10.1021/acs.macromol.8b00994
Macromolecules 2018, 51, 6190−6201

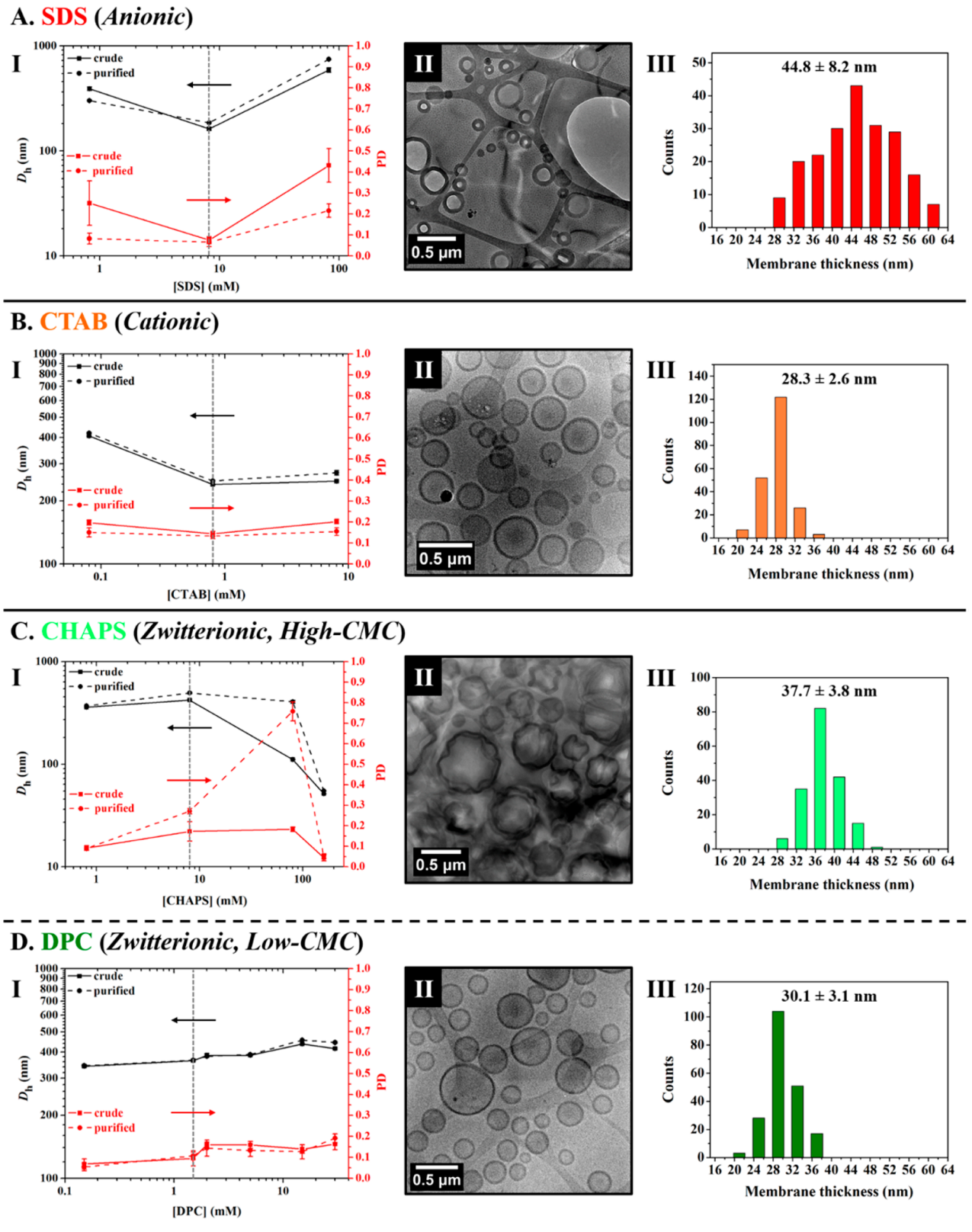

Figure 3. Summary of DLS and cryo-TEM analyses results for PEG_{113}-*b*-$PHPMA_{400}$ diblock copolymer nano-objects prepared by aqueous photo-PISA in the presence of ionic surfactants SDS (anionic) (A) and CTAB (cationic) (B) and zwitterionic surfactants CHAPS (C) and DPC (D). For each individual surfactant: (I) DLS of crude and purified formulations for the monitoring of D_h and PD changes upon increasing surfactant concentration (the error shows the standard deviation from five repeat measurements, while the vertical dashed line indicates the CMC value of each detergent). (II) Representative cryo-TEM images of purified PEG_{113}-*b*-$PHPMA_{400}$ nano-objects formed at C_{surf} = CMC. (III) Distribution of vesicles' membrane thicknesses measured from statistical analysis and calculated average membrane thickness (the error shows the standard deviation from at least 150 particle membranes).

DOI: 10.1021/acs.macromol.8b00994
Macromolecules 2018, 51, 6190−6201

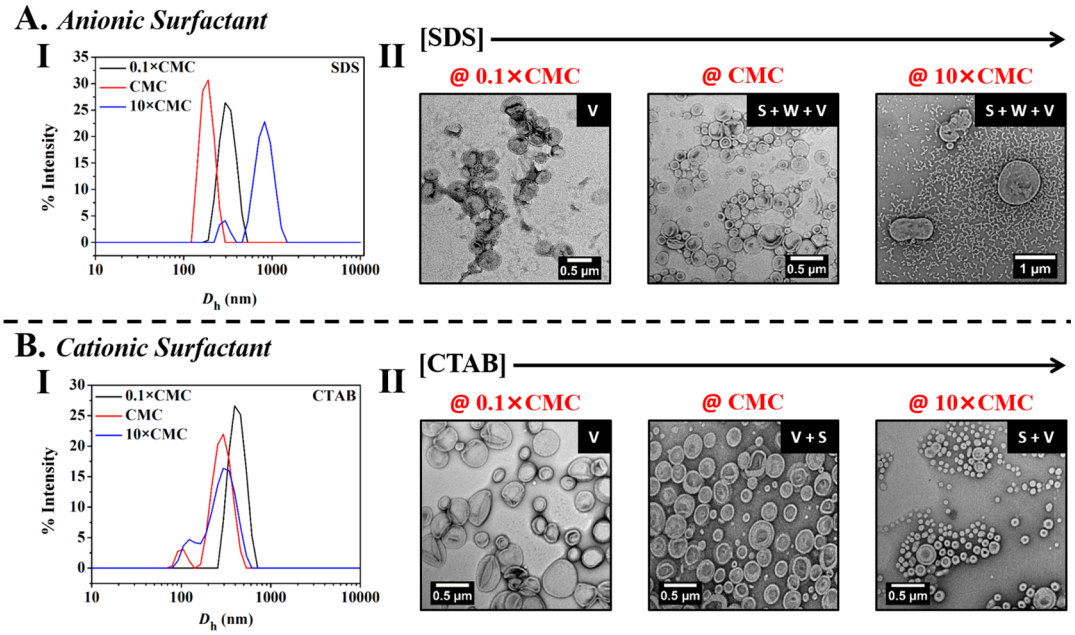

Figure 4. DLS analyses and dry-state TEM imaging results for PEG_{113}-*b*-$PHPMA_{400}$ diblock copolymer nano-objects developed by photo-PISA in aqueous solutions of anionic surfactant SDS (A) and cationic surfactant CTAB (B), upon gradually increasing C_{surf}. For each individual surfactant: (I) Intensity-weighted size distributions of purified PEG_{113}-*b*-$PHPMA_{400}$ nano-objects developed in detergent solutions of different concentrations, as determined by DLS. (II) Representative dry-state TEM micrographs of purified PEG_{113}-*b*-$PHPMA_{400}$ nano-objects formed in the presence of ionic surfactants, stained with 1 wt % UA, revealing a transition from vesicles (V) to mixed morphologies (S + W + V) upon increasing [SDS] and a direct vesicle-to-sphere morphology transition upon increasing [CTAB].

methods. It is apparent that ULVs of comparable size and membrane thickness to PEG_{113}-*b*-$PHPMA_{400}$ vesicles in DI water were formed in cases of non-ionic Triton X-100 and DDM at C_{surf} = CMC (Figures 2A-II, 2A-III, 2B-II, and 2B-III). As a matter of fact, membranes were found to be slightly thicker in both samples (average membrane thickness = 27−29 nm) compared to those in DI water, suggesting the limited insertion of surfactant molecules in the particles' hydrophobic bilayer leading to a negligible increase of average membrane thickness. On the contrary, in the case of high-CMC non-ionic surfactant OG, a significant particles' size increase from 350 to 760 nm was noticed at surfactant concentrations equal to or 10 times higher than its CMC value. In this case, the measured PD values were also found to be higher than those in the other non-ionic surfactants, ranging from 0.1 to 0.2, indicating the formation of particles with broader size distribution (Figure 2C-I). Dry-state TEM imaging at [OG] = 18.0 mM (= CMC) confirmed the formation of giant unilamellar vesicles (GULVs) of varying sizes, while TEM images at [OG] = 180.0 mM (= 10 × CMC) revealed the coexistence of GULVs along with a population of large multilamellar vesicles (MLVs) (Figures S11 and S12). As determined by cryo-TEM imaging, exceptionally large ULVs with rough outline, significantly thicker membranes (average membrane thickness ≈40 nm), and broad bilayer thickness distribution were formed in the case of exceedingly high-CMC OG at C_{surf} = CMC (Figures 2C-II and 2C-III). These findings suggest that the higher surfactant weight fraction required for the preparation of OG solutions leads to the formation of larger hybrid polymer−surfactant vesicular structures due to stronger interaction between OG molecules and vesicle membranes that aids chain mobility and exchange, thereby allowing larger vesicles to form. However, the significantly lower relative amount of surfactant needed for the preparation of Triton X-100 and DDM solutions is not able to strongly affect the size or the interfacial curvature of PEG_{113}-*b*-$PHPMA_{400}$ vesicles. The evidently high tolerance of photo-PISA toward non-ionic surfactant species is also in agreement with relevant literature reports on polymer/surfactant assemblies, supporting that there is no or limited interaction between non-ionic small molecule surfactants and neutral polymer structures.[8,10]

Photo-PISA Nano-Objects Developed in the Presence of Ionic Surfactants. In the case of commonly used high-CMC anionic surfactant SDS, DLS measurements showed significant size and PD differences and coexistence of mixed populations for the developed nano-objects upon increasing detergent concentration (Figures 3A-I and 4A-I). The corresponding hydrodynamic diameter of particles was similar to that of vesicles in DI water only at [SDS] = 0.82 mM (= 0.1 × CMC), while the observed variations of D_h and PD values at [SDS] ≥ CMC indicate strong surfactant interaction with the copolymer chains and the occurrence of morphological transitions. In particular, dry-state TEM imaging verified the development of spherical ULVs around 350−420 nm at low SDS concentration (Figure 4A-II and Figure S13). In contrast, photo-PISA at [SDS] = 8.2 mM (= CMC) resulted in the formation of mixed morphologies of spherical micelles, short worms, and ULVs of various sizes, as judged by dry-state and cryo-TEM imaging, due to greater interaction of surfactant molecules with the block copolymer chains leading to interfacial curvature changes (Figures 3A-II and 4A-II, Figure S14). In this case, the average membrane thickness of vesicles was calculated to be around 45 nm and was remarkably higher compared to that of vesicles in DI water (Figure 3A-III). A 10-fold surfactant concentration increase to [SDS] = 82.0 mM further promoted the surfactant-induced dissociation of polymer/surfactant assemblies toward lower-order structures. Dry-state TEM imaging showed a significant increase in the

DOI: 10.1021/acs.macromol.8b00994
Macromolecules 2018, 51, 6190−6201

worm-like and spherical micelles' population against ULVs (Figure 4A-II and Figure S15). In addition to the described results, the well-known ability of SDS to denature enzymes and other proteins makes it unsuitable candidate for enzyme-loaded nanoreactor development and amphiphile incorporation applications. On the other hand, for cationic surfactant CTAB, a direct vesicle-to-sphere morphology transition was observed at [CTAB] ≥ CMC, as judged by DLS and dry-state TEM analyses. DLS measurements of crude and purified samples for removal of unbound detergent revealed a significant D_h decrease from 400 to 250 nm upon increasing CTAB concentration, while PD values were constantly in the range 0.15−0.2 (Figure 3B-I). DLS size distributions showed the presence of two particle populations for small spherical micelles and vesicles at [CTAB] ≥ 0.8 mM, while a single population of vesicles was detected at low CTAB concentration (Figure 4B-I). DLS results were also verified by dry-state TEM imaging of purified samples at different surfactant concentrations. Unilamellar vesicles identical to those formed in DI water were solely observed at [CTAB] = 0.08 mM (= 0.1 × CMC) (Figure 4B-II and Figure S16), while the formation of spheres as well as small and large ULVs was revealed at [CTAB] = CMC (Figure 4B-II and Figure S17). Cryo-TEM imaging at this CTAB concentration also confirmed the coexistence of a mixture of very small and larger ULVs, while an average bilayer thickness of around 28 nm, similar to that of low-CMC non-ionic surfactant samples, was measured from digital image analysis (Figures 3B-II and 3B-III). A further increase of [CTAB] from 0.8 to 8.0 mM (= 10 × CMC) favored the formation of spherical micelles; hence, the population of spheres was notably larger than that of vesicles in this case (Figure 4B-II and Figure S18). This could be explained by the gradual introduction of positive charges, caused by the increasing [CTAB], that blend into the diblock copolymer chains developing strong repulsive forces and leading to dissociation of vesicles in favor of spheres (i.e., significant increase of interfacial curvature). It should also be mentioned that complete charge screening occurred at [CTAB] = 8.0 mM (measured zeta potential = −1.25 ± 0.32 mV), owing to neutralization of the negative vesicles' charge by the positively charged surfactant molecules. For both ionic surfactants, comparable findings were also discussed by Armes' group in a different study and are mainly attributed to the high sensitivity of RAFT-mediated PISA to the presence of ionic molecules, which makes it more difficult to obtain higher-order morphologies in contrast to the less-disruptive non-ionic surfactants.[10,52] The greater disruptive power of anionic surfactant SDS as compared to that of cationic CTAB is mainly attributed to the greater molar concentration for a given mass concentration of the former (i.e., CMC_{SDS} > CMC_{CTAB}).[10]

Photo-PISA Nano-Objects Developed in the Presence of Zwitterionic Surfactants. Importantly, the effect of two model zwitterionic (ampholytic) surfactants on PEG_{113}-*b*-$PHPMA_{400}$ photo-PISA nano-object formulations was thoroughly investigated. In the case of high-CMC steroid surfactant CHAPS, slight size differences were observed at low surfactant concentrations (i.e., [CHAPS] ≤ CMC), as judged by DLS (Figure 3C-I). However, a dramatic D_h decrease from 420 to 110 nm was observed at [CHAPS] = 80.0 mM (= 10 × CMC) (PD = 0.18, zeta potential = −15.6 ± 0.3 mV), while further [CHAPS] increase to 160.0 mM (= 20 × CMC) resulted in a notable D_h decrease to almost 50 nm (PD = 0.04, zeta potential = −10.4 ± 1.9 mV), indicating the occurrence of morphological transitions from ULVs to lower-order structures upon increasing detergent concentration. Interestingly, dry-state TEM imaging revealed a morphologically distinct vesicle-to-worm-to-sphere transition upon increasing [CHAPS] from CMC to 10 × CMC and subsequently to 20 × CMC (Figure 5A and Figures S19−S21). ULVs of uniform shape and size with significantly thicker hydrophobic membranes (average membrane thickness ≈38 nm) and rough outline were formed at [CHAPS] = 8.0 mM (= CMC), as shown by cryo-TEM (Figures 3C-II and 3C-III), whereas a pure network of branched worms was apparently observed after photo-PISA in 80.0 mM CHAPS solution. This was initially indicated on a macroscopic level by the formation a free-standing gel in the reaction vial after the polymerization process. The increase of both D_h and PD noticed in this sample after purification is mainly attributed to further entanglement of the worm-like micelles during the centrifugation/resuspension process.[24] Additional dry-state TEM imaging at [CHAPS] = 160.0 mM clearly showed the development of small spherical micelles, confirming the results received from DLS analysis. As ^{1}H NMR spectroscopy suggested that only 70% monomer consumption occurred after 2 h of reaction in this sample, an overnight photo-PISA reaction was repeated to ensure full monomer conversion. In this case, dry-state TEM imaging showed the formation of mostly small spherical micelles along with some short worms, derived from the integration of adjacent spheres (Figure S22). Similar to the studied ionic surfactants, it is evident that the presence of high amounts of charged zwitterionic surfactant molecules promotes their ionic-like behavior and markedly affects the photo-

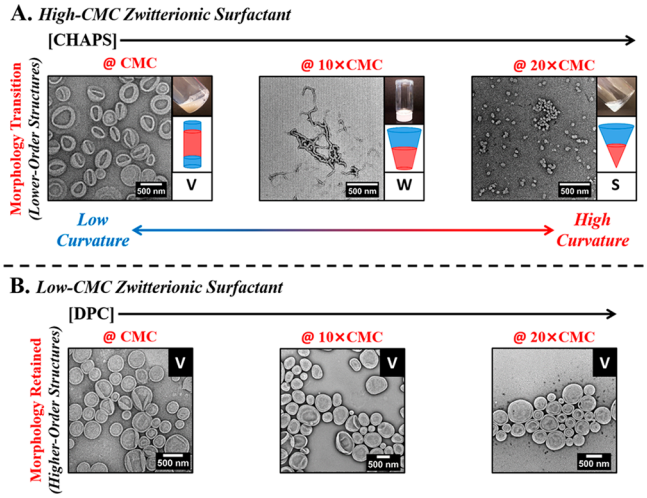

Figure 5. (A) Representative dry-state TEM micrographs, stained with 1 wt % UA, reaction vial images, and illustrations of the interfacial curvature of PEG_{113}-*b*-$PHPMA_{400}$ nano-objects developed by aqueous photo-PISA upon increasing concentration of high-CMC zwitterionic surfactant CHAPS. A vesicle-to-worm morphology transition is observed at [CHAPS] = 10 × CMC, while a subsequent worm-to-sphere transition is noticed at [CHAPS] = 20 × CMC. (B) Representative dry-state TEM micrographs, stained with 1 wt % UA, of PEG_{113}-*b*-$PHPMA_{400}$ nano-objects developed by aqueous photo-PISA upon increasing concentration of low-CMC zwitterionic surfactant DPC. No morphology transitions were observed; hence, ULVs of comparable sizes were achieved at concentrations ranging from [DPC] = CMC to 20 × CMC.

DOI: 10.1021/acs.macromol.8b00994
Macromolecules 2018, 51, 6190−6201

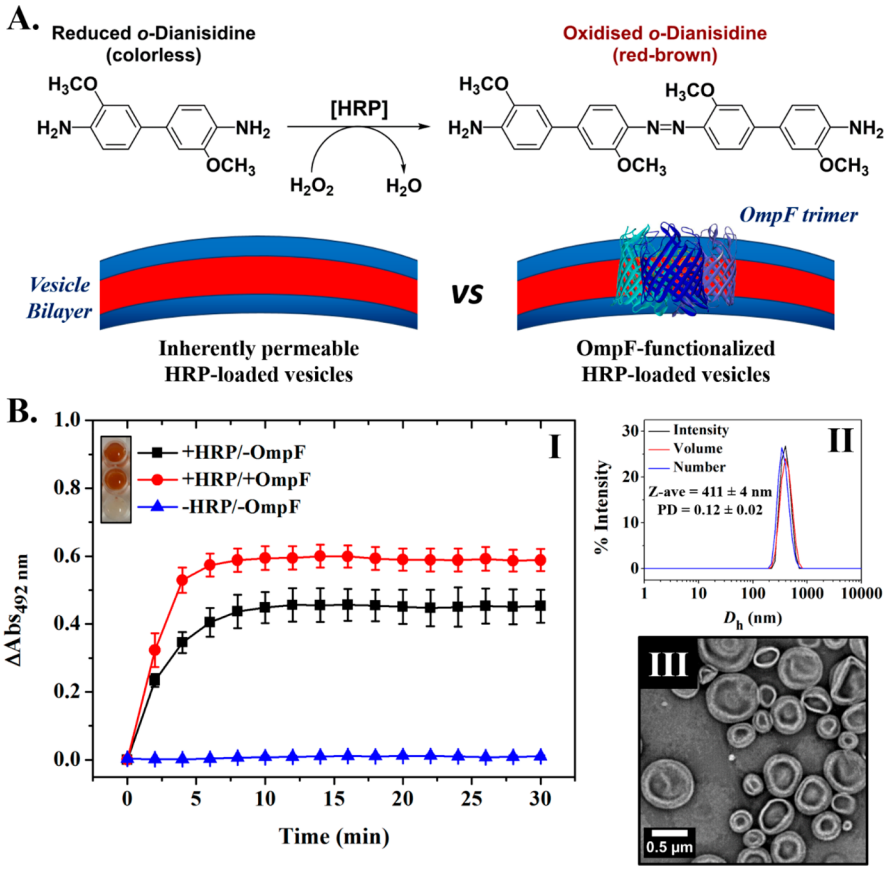

Figure 6. (A) HRP-catalyzed oxidation reaction of *o*-dianisidine to a red-brown dimer product, detected by colorimetric assay, taking place inside inherently permeable HRP-loaded PEG_{113}-*b*-$PHPMA_{400}$ vesicles and OmpF-functionalized + HRP-loaded PEG_{113}-*b*-$PHPMA_{400}$ vesicles. (B) Enzymatic activity of the purified empty (−HRP/−OmpF, blue line), HRP-loaded (+HRP/−OmpF, black line), and OmpF-functionalized + HRP-loaded (+HRP/+OmpF, red line) PEG_{113}-*b*-$PHPMA_{400}$ vesicles at 0.5 wt % (the inset shows the end-point microwells in each case) (I), intensity-weighted size distributions of purified OmpF-functionalized + HRP-loaded PEG_{113}-*b*-$PHPMA_{400}$ vesicles obtained by DLS, along with the average D_h and PD values (the error shows the standard deviation from five repeat measurements) (II), and representative dry-state TEM image, stained with 1 wt % UA (III).

PISA process, preventing the formation of higher-order structures. The incorporation of zwitterionic detergent molecules into the bilayer of the assemblies combined with the introduction of charges in the hydrophilic corona of the nano-objects drives the development of mixed polymer−surfactant formulations with higher interfacial curvature (i.e., transitions to worm-like or spherical micelles). Above all, pure phases of ULVs, worms, and spherical micelles were isolated by careful control of CHAPS concentration during aqueous photo-PISA of the same block copolymer. Surprisingly, in the case of the other studied zwitterionic phospholipid surfactant DPC, completely opposite behavior compared to high-CMC CHAPS and analogous to that of non-ionic and low-CMC detergents Triton X-100 and DDM was observed. In particular, minor size and PD variations were recorded for a wide range of DPC concentrations, in comparison to original PEG_{113}-*b*-$PHPMA_{400}$ ULVs in DI water, suggesting that no dissociation to lower-order constructs occurred in this case, even at extreme detergent concentrations (Figure 3D-I). The hydrodynamic diameter of photo-PISA samples in DPC solutions ranged between 340 nm for low [DPC] and 440 nm for higher [DPC], while low PD values of 0.07−0.15 were also measured. It should also be noted that in the case of DPC the purification process did not affect the D_h or PD values. Dry-state and cryo-TEM imaging at [DPC] = 1.5 mM (= CMC) revealed the successful development of pure spherical ULVs of uniform size (Figures 3D-II and 5B, Figure S23). Based on cryo-TEM analysis, the average membrane thickness of vesicles formed at [DPC] = CMC was determined to be around 30 nm (Figure 3D-III). This indicates negligible interaction between DPC molecules and polymeric chains, following the same trend as low-CMC non-ionic surfactants. Additionally, the vesicular morphology and unilamellar character were retained upon increasing DPC concentration up to 20 times above its CMC value, showing the high tolerance of photo-PISA toward this particular surfactant (Figure 5B, Figures S24 and S25). The marked differences observed between the two zwitterionic detergents are attributed to the higher weight percent of surfactant required in the case of CHAPS ($CMC_{CHAPS} > CMC_{DPC}$), revealing the dual nature of such species that are possible to behave like non-ionic or ionic surfactants depending on the conditions. Finally, these findings are of paramount importance as it was demonstrated that besides neutral detergents, an ampholytic small molecule surfactant could also be used for applications of biorelevant interest without drastically affecting the desired final morphologies prepared by aqueous PISA. The observed morphologies of all formulations developed by RAFT-mediated photo-PISA in aqueous surfactant solutions, as

DOI: 10.1021/acs.macromol.8b00994
Macromolecules 2018, 51, 6190−6201

judged by dry-state and cryo-TEM, are summarized in Table S3.

Outer Membrane Protein F (OmpF) Reconstitution into PEG_{113}-*b*-$PHPMA_{400}$ Vesicles. Guided by the results on the tolerance of PISA to surfactants, a challenging functional membrane protein, which is not soluble in aqueous media in the absence of surfactants, was selected for incorporation during the photo-PISA process. The channel-forming membrane protein OmpF trimer was extracted from *Escherichia coli* (see the Supporting Information), purified, and stabilized in an aqueous surfactant solution mixture of 0.39 mM DDM + 20 mM sodium phosphate (NaPhos) at pH = 6.0 (Figures S27 and S28). Initial photo-PISA reactions for the synthesis of PEG_{113}-*b*-$PHPMA_{400}$ block copolymers in 20 mM NaPHos and 0.39 mM DDM + 20 mM NaPHos solutions (pH = 6.0) in the absence of OmpF protein revealed that the controlled polymerization character ($Đ_M$ ca. = 1.3, monomer conversion >98%) and original vesicular morphology were retained in both cases, with negligible D_h and membrane thickness increases being observed (Figures S29 and S30). Importantly, 405 nm irradiation of DDM-stabilized OmpF for 2 h did not affect the secondary structure and hence functionality of the protein, as judged by circular dichroism (CD) measurements before and after light exposure (Figure S31). These findings suggest that by using this particular surfactant solution, OmpF could be directly reconstituted into the inherently permeable PHPMA membrane of vesicles by photo-PISA. Horseradish peroxidase (HRP) was chosen to be encapsulated into the lumen of both −OmpF and +OmpF-containing ULVs to provide a read-out of function of OmpF (permeability) by kinetic colorimetric assays, following a recently reported procedure by our group.[36] HRP catalyzes the oxidation reaction of the colorless substrate *o*-dianisidine to the colored (red-brown) dimer product, which can be detected by measuring the absorbance at λ = 492 nm over time (Figure 6A). The surfactant-stabilized OmpF protein was reconstituted into HRP-loaded ULVs by a one-pot photo-PISA reaction to introduce nonselective channels that would allow easier exchange of small molecules between the aqueous compartments of particles. From kinetic colorimetric analyses, a noticeable absorbance increase of 24 ± 3% was measured in the case of purified +OmpF-containing ULVs compared to −OmpF ones, demonstrating the permeability enhancement of the former toward *o*-dianisidine and hydrogen peroxide and OmpF retention of function (Figure 6B-I). A similar permeability enhancement was also monitored upon ranging the particles' concentration from 0.5 to 0.1 wt % during kinetic colorimetric analyses. Dry-state TEM imaging confirmed the formation of OmpF-functionalized + HRP-loaded ULVs, while additional DLS analysis showed a negligible D_h increase to 411 ± 4 nm, similar to that observed in DDM + NaPhos mixture without OmpF (Figures 6B-II and 6B-III and Figure S32).

CONCLUSIONS

In this study, an insight into the effect of different types of small molecule surfactants on aqueous photoinitiated PISA processes for the formation of polymer/surfactant complex nano-objects was explored. Investigation revealed the high tolerance of photo-PISA toward non-ionic surfactants with varying CMC values, as the originally targeted vesicular morphology was consistently retained in these cases. On the contrary, the high sensitivity of photo-PISA to the presence of ionic species was verified by the occurrence of morphological transitions toward lower-order structures upon increasing concentration of ionic surfactants. The introduction of charged molecules into the polymeric chains markedly affected the self-assembly process, leading to the development of formulations with larger interfacial curvatures. Moreover, the presence of zwitterionic surfactants of high or low CMC values was also studied. An interesting vesicle-to-worm-to-sphere morphology transition was observed upon increasing concentration of high-CMC zwitterionic surfactant, while in the case of low-CMC detergent vesicular structures similar to those developed in non-ionic surfactant solutions were formed at a wide range of concentrations. By using these results as a guide, a low-CMC non-ionic surfactant was selected for the stabilization/solublization of the hydrophobic channel-forming membrane protein OmpF, which was then able to be reconstituted into the membrane of the vesicles by a one-pot photo-PISA process. This highlights the robustness of photo-PISA for the *in situ* insertion of delicate non-stable hydrophobic species to allow for the facile synthesis of biomimetic nanoreactors.

METHODS

Materials and Methods. Materials and characterization techniques used are included in the Supporting Information. The syntheses of 4-cyano-4-[(ethylsulfanylthiocarbonyl)sulfanyl]pentanoic acid chain transfer agent (CEPA CTA) and poly(ethylene glycol)$_{113}$−CEPA macro-CTA (PEG_{113}−CEPA mCTA) by *N*,*N*′-dicyclohexylcarbodiimide (DCC) coupling between PEG_{113} monomethyl ether and CEPA CTA were performed according to previously described processes with slight modification.[24,53] The synthetic procedures followed are given in detail in the Supporting Information. All photo-PISA reactions were performed in a custom-built photoreactor setup. This ensured the reaction mixture was only exposed to the light from the 400−410 nm LED source placed underneath the sample.

Synthesis of PEG_{113}-*b*-$PHPMA_{400}$ Diblock Copolymer Nano-Objects by Aqueous Photoinitiated Polymerization-Induced Self-Assembly (Photo-PISA) in Surfactant Solutions. A typical synthetic procedure to achieve PEG_{113}-*b*-$PHPMA_{400}$ diblock copolymer nano-objects at 10 wt % HPMA (or 11% solids content) by aqueous RAFT-mediated photo-PISA is described (Scheme S1).[24] PEG_{113}−CEPA mCTA (9.1 mg, 1.7 μmol, 1 equiv) and HPMA (100 mg, 0.69 mmol, 400 equiv) were dissolved in a freshly prepared aqueous surfactant solution of desired concentration (0.9 mL) in a sealed 20 mL scintillation vial bearing a magnetic stirrer bar. The resulting polymerization solution was degassed by purging with N_2(g) for 15 min. The sealed vial was incubated at 37 °C with magnetic stirring under 405 nm light irradiation for 2 h to ensure full monomer conversion. After this period, the reaction mixture was exposed to air and allowed to cool to room temperature before conversion ^{1}H NMR and SEC analyses. The resulting solution of particles was then diluted 10-fold in DI water and purified by three centrifugation/resuspension cycles in DI water at 14000 rpm for the removal of unreacted monomer and/or excess of non-incorporated surfactant molecules (Figure S1). ^{1}H NMR in methanol-d_4 and DMF SEC traces of the pure polymer were obtained after lyophilization of an aliquot of particles. TEM, DLS, and zeta potential analyses were performed on samples after dilution to an appropriate analysis concentration.

HRP Loading and OmpF Reconstitution into PEG_{113}-*b*-$PHPMA_{400}$ Vesicles by Aqueous Photo-PISA. For the synthesis of permeable non-OmpF-containing HRP-loaded PEG_{113}-*b*-$PHPMA_{400}$ vesicles at 10 wt % HPMA by aqueous photo-PISA, a previously reported procedure was followed.[36] For the reconstitution of OmpF porin, PEG_{113}−CEPA mCTA (9.1 mg, 1.7 μmol, 1 equiv) and HPMA (100 mg, 0.69 mmol, 400 equiv) were first dissolved in DI water (0.53 mL) in a sealed 20 mL scintillation vial bearing a magnetic stirrer bar. Once homogeneous, 0.1 mL of a 200 U mL^{-1} HRP solution in DI water and 0.27 mL of a 750 μg mL^{-1} OmpF solution in 0.39 mM DDM + 20 mM NaPhos (pH = 6.0) were added. The resulting polymerization solution was degassed by purging with N_2(g) for 15

DOI: 10.1021/acs.macromol.8b00994
Macromolecules 2018, 51, 6190−6201

min. The sealed vial was incubated at 37 °C with magnetic stirring under 405 nm light irradiation for 2 h to ensure full monomer conversion. After this period, the reaction mixture was exposed to air and allowed to cool to room temperature before conversion ^{1}H NMR, kinetic colorimetric, and microscopic analyses. The resulting solutions of non-OmpF and OmpF-containing particles were then diluted 10-fold in 100 mM PB (pH = 5.5) and purified by three centrifugation/resuspension cycles in 100 mM PB (pH = 5.5) at 14000 rpm for the removal of unreacted monomer, free HRP enzyme, and/or non-incorporated OmpF molecules.

■ ASSOCIATED CONTENT

Supporting Information

The Supporting Information is available free of charge on the ACS Publications website at DOI: 10.1021/acs.macromol.8b00994.

Materials and characterization techniques, experimental details, additional SEC eluograms of PEG_{113}-*b*-$PHPMA_{400}$ diblock copolymers synthesized in DI water and various surfactant solutions, additional dry-state TEM and cryo-TEM images of nano-objects, OmpF reconstitution supplementary data (PDF)

■ AUTHOR INFORMATION

Corresponding Author

*E-mail: r.oreilly@bham.ac.uk.

ORCID

Eamonn Reading: 0000-0001-8219-0052
Matthew I. Gibson: 0000-0002-8297-1278
Rachel K. O'Reilly: 0000-0002-1043-7172

Notes

The authors declare no competing financial interest.

■ ACKNOWLEDGMENTS

This work was supported by the ERC (638661, 294342, and 615142), EPSRC, and University of Warwick. Dr. E. Reading is funded by BBSRC Future Leader Fellowship BB/N011201/1. Dr. S. Bakker and Mr. R. Keogh (University of Warwick) are thanked for cryo-TEM assistance, and Advanced BioImaging Research Technology Platform, BBSRC ALERT14 award BB/M01228X/1, is thanked for supporting cryo-TEM characterization. Dr. M. Hasan (University of Warwick) is thanked for CD assistance.

■ REFERENCES

(1) Karsa, D. R. *Industrial Applications of Surfactants IV*; The Royal Society of Chemistry: Cambridge, 1999.

(2) Schramm, L. L. *Surfactants: Fundamentals and Applications in the Petroleum Industry*; Cambridge University Press: Cambridge, 2000.

(3) Blanazs, A.; Armes, S. P.; Ryan, A. J. Self-Assembled Block Copolymer Aggregates: From Micelles to Vesicles and their Biological Applications. Macromol. *Macromol. Rapid Commun.* **2009**, *30*, 267–277.

(4) Chang, H.-Y.; Sheng, Y.-H.; Tsao, H.-K. Structural and Mechanical Characteristics of Polymersomes. *Soft Matter* **2014**, *10*, 6373–6381.

(5) Banerjee, S.; Cazeneuve, C.; Baghdadli, N.; Ringeissen, S.; Leermakers, F. A. M.; Luengo, G. S. Surfactant-Polymer Interactions: Molecular Architecture Does Matter. *Soft Matter* **2015**, *11*, 2504–2511.

(6) Holmberg, K.; Jönsson, B.; Kronberg, B.; Lindman, B. *Surfactants and Polymers in Aqueous Solution*, 2nd ed.; John Wiley & Sons, Ltd.: West Sussex, 2003.

(7) Wesley, R.; Cosgrove, T.; Thompson, L.; Armes, S. P.; Baines, F. L. Structure of Polymer/Surfactant Complexes Formed by Poly(2-(dimethylamino)ethyl methacrylate) and Sodium Dodecyl Sulfate. *Langmuir* **2002**, *18*, 5704–5707.

(8) Diamant, H.; Andelman, D. Onset of Self-Assembly in Polymer-Surfactant Systems. *Europhys. Lett.* **1999**, *48*, 170–176.

(9) Pata, V.; Ahmed, F.; Discher, D. E.; Dan, N. Membrane Solubilization by Detergent: Resistance Conferred by Thickness. *Langmuir* **2004**, *20*, 3888–3893.

(10) Chambon, P.; Blanazs, A.; Battaglia, G.; Armes, S. P. How Does Cross-Linking Affect the Stability of Block Copolymer Vesicles in the Presence of Surfactant? *Langmuir* **2012**, *28*, 1196–1205.

(11) Atanase, L. I.; Lerch, J.-P.; Caprarescu, S.; Iurciuc, C. E.; Riess, G. Micellization of pH-Sensitive Poly(butadiene)-*block*-poly(2 vinylpyridine)-*block*-poly(ethylene oxide) Triblock Copolymers: Complex Formation with Anionic Surfactants. *J. Appl. Polym. Sci.* **2017**, *134*, 45313.

(12) Nam, J.; Beales, P. A.; Vanderlick, T. K. Giant Phospholipid/Block Copolymer Hybrid Vesicles: Mixing Behavior and Domain Formation. *Langmuir* **2011**, *27*, 1–6.

(13) Nam, J.; Vanderlick, T. K.; Beales, P. A. Formation and Dissolution of Phospholipid Domains with Varying Textures in Hybrid Lipo-Polymersomes. *Soft Matter* **2012**, *8*, 7982–7988.

(14) Le Meins, J.-F.; Schatz, C.; Lecommandoux, S.; Sandre, O. Hybrid Polymer/Lipid Vesicles: State of the Art and Future Perspectives. Mater. *Mater. Today* **2013**, *16*, 397–402.

(15) Schulz, M.; Binder, W. H. Mixed Hybrid Lipid/Polymer Vesicles as a Novel Membrane Platform. Macromol. *Macromol. Rapid Commun.* **2015**, *36*, 2031–2041.

(16) Warren, N. J.; Armes, S. P. Polymerization-Induced Self-Assembly of Block Copolymer Nano-objects via RAFT Aqueous Dispersion Polymerization. *J. Am. Chem. Soc.* **2014**, *136*, 10174–10185.

(17) Canning, S. L.; Smith, G. N.; Armes, S. P. A Critical Appraisal of RAFT-Mediated Polymerization-Induced Self-Assembly. *Macromolecules* **2016**, *49*, 1985–2001.

(18) Karagoz, B.; Boyer, C.; Davis, T. P. Simultaneous Polymerization-Induced Self-Assembly (PISA) and Guest Molecule Encapsulation. *Macromol. Rapid Commun.* **2014**, *35*, 417–421.

(19) Zhou, W.; Qu, Q.; Xu, Y.; An, Z. Aqueous Polymerization-Induced Self-Assembly for the Synthesis of Ketone-Functionalized Nano-Objects with Low Polydispersity. *ACS Macro Lett.* **2015**, *4*, 495–499.

(20) Qiao, X. G.; Dugas, P.-Y.; Charleux, B.; Lansalot, M.; Bourgeat-Lami, E. Nitroxide-Mediated Polymerization-Induced Self-Assembly of Amphiphilic Block Copolymers with a pH/Temperature Dual Sensitive Stabilizer Block. *Polym. Chem.* **2017**, *8*, 4014–4029.

(21) Wang, G.; Schmitt, M.; Wang, Z.; Lee, B.; Pan, X.; Fu, L.; Yan, J.; Li, S.; Xie, G.; Bockstaller, M. R.; Matyjaszewski, K. Polymerization-Induced Self-Assembly (PISA) Using ICAR ATRP at Low Catalyst Concentration. *Macromolecules* **2016**, *49*, 8605–8615.

(22) Blanazs, A.; Madsen, J.; Battaglia, G.; Ryan, A. J.; Armes, S. P. Mechanistic Insights for Block Copolymer Morphologies: How Do Worms Form Vesicles? *J. Am. Chem. Soc.* **2011**, *133*, 16581–16587.

(23) Williams, M.; Penfold, N. J. W.; Lovett, J. R.; Warren, N. J.; Douglas, C. W. I.; Doroshenko, N.; Verstraete, P.; Smets, J.; Armes, S. P. Bespoke Cationic Nano-Objects via RAFT Aqueous Dispersion Polymerization. *Polym. Chem.* **2016**, *7*, 3864–3873.

(24) Blackman, L. D.; Doncom, K. E. B.; Gibson, M. I.; O'Reilly, R. K. Comparison of Photo- and Thermally Initiated Polymerization-Induced Self-Assembly: A Lack of End Group Fidelity Drives the Formation of Higher Order Morphologies. *Polym. Chem.* **2017**, *8*, 2860–2871.

(25) Figg, C. A.; Carmean, R. N.; Bentz, K. C.; Mukherjee, S.; Savin, D. A.; Sumerlin, B. S. Tuning Hydrophobicity To Program Block Copolymer Assemblies from the Inside Out. *Macromolecules* **2017**, *50*, 935–943.

(26) Derry, M. J.; Fielding, L. A.; Armes, S. P. Polymerization-Induced Self-Assembly of Block Copolymer Nanoparticles via RAFT

DOI: 10.1021/acs.macromol.8b00994
Macromolecules 2018, 51, 6190–6201

Non-Aqueous Dispersion Polymerization. *Prog. Polym. Sci.* **2016**, *52*, 1−18.
(27) Yeow, J.; Boyer, C. Photoinitiated Polymerization-Induced Self-Assembly (Photo-PISA): New Insights and Opportunities. *Adv. Sci.* **2017**, *4*, 1700137.
(28) Tan, J.; Sun, H.; Yu, M.; Sumerlin, B. S.; Zhang, L. Photo-PISA: Shedding Light on Polymerization-Induced Self-Assembly. *ACS Macro Lett.* **2015**, *4*, 1249−1253.
(29) Yeow, J.; Xu, J.; Boyer, C. Polymerization-Induced Self-Assembly Using Visible Light Mediated Photoinduced Electron Transfer−Reversible Addition−Fragmentation Chain Transfer Polymerization. *ACS Macro Lett.* **2015**, *4*, 984−990.
(30) Tan, J.; Bai, Y.; Zhang, X.; Zhang, L. Room Temperature Synthesis of Poly(poly(ethylene glycol) methyl ether methacrylate)-Based Diblock Copolymer Nano-Objects via Photoinitiated Polymerization-Induced Self-Assembly (Photo-PISA). *Polym. Chem.* **2016**, *7*, 2372−2380.
(31) Tan, J.; Liu, D.; Bai, Y.; Huang, C.; Li, X.; He, J.; Xu, Q.; Zhang, X.; Zhang, L. An Insight into Aqueous Photoinitiated Polymerization-Induced Self-Assembly (photo-PISA) for the Preparation of Diblock Copolymer Nano-Objects. *Polym. Chem.* **2017**, *8*, 1315−1327.
(32) Sadrearhami, Z.; Yeow, J.; Nguyen, T.-K.; Ho, K. K. K.; Kumar, N.; Boyer, C. Biofilm Dispersal Using Nitric Oxide Loaded Nanoparticles Fabricated by Photo-PISA: Influence of Morphology. *Chem. Commun.* **2017**, *53*, 12894−12897.
(33) Tan, J.; Li, X.; Zeng, R.; Liu, D.; Xu, Q.; He, J.; Zhang, Y.; Dai, X.; Yu, L.; Zeng, Z.; Zhang, L. Expanding the Scope of Polymerization-Induced Self-Assembly: Z-RAFT-Mediated Photoinitiated Dispersion Polymerization. *ACS Macro Lett.* **2018**, *7*, 255−262.
(34) Tan, J.; Liu, D.; Huang, C.; Li, X.; He, J.; Xu, Q.; Zhang, L. Photoinitiated Polymerization-Induced Self-Assembly of Glycidyl Methacrylate for the Synthesis of Epoxy-Functionalized Block Copolymer Nano-Objects. Macromol. *Macromol. Rapid Commun.* **2017**, *38*, 1700195.
(35) Tan, J.; Liu, D.; Bai, Y.; Huang, C.; Li, X.; He, J.; Xu, Q.; Zhang, L. Enzyme-Assisted Photoinitiated Polymerization-Induced Self-Assembly: An Oxygen-Tolerant Method for Preparing Block Copolymer Nano-Objects in Open Vessels and Multiwell Plates. *Macromolecules* **2017**, *50*, 5798−5806.
(36) Blackman, L. D.; Varlas, S.; Arno, M. C.; Fayter, A.; Gibson, M. I.; O'Reilly, R. K. Permeable Protein-Loaded Polymersome Cascade Nanoreactors by Polymerization-Induced Self-Assembly. *ACS Macro Lett.* **2017**, *6*, 1263−1267.
(37) Tan, J.; Zhang, X.; Liu, D.; Bai, Y.; Huang, C.; Li, X.; Zhang, L. Facile Preparation of CO_2-Responsive Polymer Nano-Objects via Aqueous Photoinitiated Polymerization-Induced Self-Assembly (Photo-PISA). *Macromol. Rapid Commun.* **2017**, *38*, 1600508.
(38) Blackman, L. D.; Varlas, S.; Arno, M. C.; Houston, Z. H.; Fletcher, N. L.; Thurecht, K. J.; Hasan, M.; Gibson, M. I.; O'Reilly, R. K. Confinement of Therapeutic Enzymes in Selectively Permeable Polymer Vesicles by Polymerization-Induced Self-Assembly (PISA) Reduces Antibody Binding and Proteolytic Susceptibility. *ACS Cent. Sci.* **2018**, *4*, 718−723.
(39) Mastrotto, F.; Breen, A. F.; Sicilia, G.; Murdan, S.; Johnstone, A. D.; Marsh, G. E.; Grainger-Boultby, C.; Russell, N. A.; Alexander, C.; Mantovani, G. One-pot RAFT and Fast Polymersomes Assembly: A 'Beeline' from Monomers to Drug-Loaded Nanovectors. *Polym. Chem.* **2016**, *7*, 6714−6724.
(40) Edlinger, C.; Einfalt, T.; Spulber, M.; Car, A.; Meier, W.; Palivan, C. G. Biomimetic Strategy to Reversibly Trigger Functionality of Catalytic Nanocompartments by the Insertion of pH-Responsive Biovalves. *Nano Lett.* **2017**, *17*, 5790−5798.
(41) Iimura, N.; Sawada, K.; Ohashi, Y.; Hirata, H. Complex Formation Between Cationic Surfactants and Insoluble Drugs. *Bull. Chem. Soc. Jpn.* **1999**, *72*, 2417−2422.
(42) Seddon, A. M.; Curnow, P.; Booth, P. J. Membrane Proteins, Lipids and Detergents: Not Just a Soap Opera. *Biochim. Biophys. Acta, Biomembr.* **2004**, *1666*, 105−117.
(43) Privé, G. G. Detergents for the Stabilization and Crystallization of Membrane Proteins. *Methods* **2007**, *41*, 388−397.
(44) Tehrani-Bagha, A. R.; Holmberg, K. Solubilization of Hydrophobic Dyes in Surfactant Solutions. *Materials* **2013**, *6*, 580−608.
(45) Tanner, P.; Onaca, O.; Balasubramanian, V.; Meier, W.; Palivan, C. G. Enzymatic Cascade Reactions Inside Polymeric Nanocontainers: A Means to Combat Oxidative Stress. *Chem. - Eur. J.* **2011**, *17*, 4552−4560.
(46) Einfalt, T.; Goers, R.; Dinu, I. A.; Najer, A.; Spulber, M.; Onaca-Fischer, O.; Palivan, C. G. Stimuli-Triggered Activity of Nanoreactors by Biomimetic Engineering Polymer Membranes. *Nano Lett.* **2015**, *15*, 7596−7603.
(47) Warren, N. J.; Mykhaylyk, O. O.; Mahmood, D.; Ryan, A. J.; Armes, S. P. RAFT Aqueous Dispersion Polymerization Yields Poly(ethylene glycol)-Based Diblock Copolymer Nano-Objects with Predictable Single Phase Morphologies. *J. Am. Chem. Soc.* **2014**, *136*, 1023−1033.
(48) Otsu, T. Iniferter Concept and Living Radical Polymerization. *J. Polym. Sci., Part A: Polym. Chem.* **2000**, *38*, 2121−2136.
(49) Lovett, J. R.; Warren, N. J.; Armes, S. P.; Smallridge, M. J.; Cracknell, R. B. Order-Order Morphological Transitions for Dual Stimulus Responsive Diblock Copolymer Vesicles. *Macromolecules* **2016**, *49*, 1016−1025.
(50) Stiufiuc, R.; Iacovita, C.; Nicoara, R.; Stiufiuc, G.; Florea, A.; Achim, M.; Lucaciu, C. M. One-Step Synthesis of PEGylated Gold Nanoparticles with Tunable Surface Charge. *J. Nanomater.* **2013**, *2013*, 1−7.
(51) Knecht, V.; Risselada, H. J.; Mark, A. E.; Marrink, S. J. Electrophoretic Mobility Does Not Always Reflect the Charge on an Oil Droplet. *J. Colloid Interface Sci.* **2008**, *318*, 477−486.
(52) Semsarilar, M.; Ladmiral, V.; Blanazs, A.; Armes, S. P. Anionic Polyelectrolyte-Stabilized Nanoparticles via RAFT Aqueous Dispersion Polymerization. *Langmuir* **2012**, *28*, 914−922.
(53) Johnson, R. N.; Burke, R. S.; Convertine, A. J.; Hoffman, A. S.; Stayton, P. S.; Pun, S. H. Synthesis of Statistical Copolymers Containing Multiple Functional Peptides for Nucleic Acid Delivery. *Biomacromolecules* **2010**, *11*, 3007−3013.

DOI: 10.1021/acs.macromol.8b00994
Macromolecules 2018, 51, 6190−6201